Nuclear Engineering and Technology 54 (2022) 3841–3848

Contents lists available at ScienceDirect

Nuclear Engineering and Technology

journal homepage: www.elsevier.com/locate/net

Original Article

Role of modifiers on the structural, mechanical, optical and radiation protection attributes of Eu^{3+} incorporated multi constituent glasses

M.K. Komal Poojha [a], K. Marimuthu [a, *], P. Evangelin Teresa [a], Nouf Almousa [b], M.I. Sayyed [c, d]

[a] Department of Physics, The Gandhigram Rural Institute-Deemed to be University, Gandhigram, 624 302, India
[b] Department of Physics, College of Science, Princess Nourah Bint Abdulrahman University, P.O. Box 84428, Riyadh, 11671, Saudi Arabia
[c] Department of Physics, Faculty of Science, Isra University, Amman, Jordan
[d] Department of Nuclear Medicine Research, Institute for Research and Medical Consultations (IRMC), Imam Abdulrahman bin Faisal University (IAU), P.O. Box 1982, Dammam, 31441, Saudi Arabia

ARTICLE INFO

Article history:
Received 30 March 2022
Received in revised form
27 April 2022
Accepted 4 May 2022
Available online 10 May 2022

Keywords:
Multi constituent glasses
FTIR
Elastic moduli
Optical bandgap
Bonding parameters
Radiation shielding

ABSTRACT

The effect of modifiers on the optical features and radiation defying ability of the Eu^{3+} ions doped multi constituent glasses was examined. XRD has established the amorphous nature of the specimen. The presence of various functional/fundamental groups in the present glasses was analyzed through FTIR spectra. The physical, structural and elastic traits of the glasses were explored. The variation in the structural compactness of the glass structure according to the incorporated modifier was enlightened to describe their suitability for a better shielding media. For the examined glasses, the metallization criterion value varied in the range 0.613–0.692, indicating the non-metallic character of the glasses with possible nonlinear optical applications. The computed elastic moduli expose the Li-containing glass (BTLi:Eu) to be tightly packed and rigid, which is a requirement for a better shielding channel. Furthermore, the optical bandgap and the Urbach energy values are calculated based on the optical absorption spectra. The evaluated bonding parameters revealed the nature of the fabricated glasses covalent. In addition, we investigated the radiation attenuation attributes of the prepared Eu^{3+} ions doped multi constituent glasses using Phy-X software. We determined the linear attenuation coefficient (LAC) and reported the influence of the five oxides Li_2O_3, CaO, BaO, SrO, and ZnO on the LAC values. The LAC varied between 0.433 and 0.549 cm^{-1} at 0.284 MeV. The $39B_2O_3–25TeO_2–15Li_2O_3–10Na_2O–10K_2O$ $–1Eu_2O_3$ glass has a much smaller LAC than the other glasses.

1. Introduction

For the past few decades in radiation physics, optical glasses have been used as a substitute and impressive shield to protect humans from hazardous radiation. Radionuclide emits excess nuclear energy in the form of ionizing radiation as beta and gamma particles. Numerous applications of radiation sources have been found in different fields such as nuclear reactors, accelerator technologies, radiotherapy, nuclear medicine, agriculture, industries, etc., [1–6]. The continuous emission of radiation affects the worker's lungs, leading to cancer and even causing death. Hence to protect humans from harmful radiations, different shielding techniques were handled through which gamma radiation cannot penetrate. Previously, complex substances like concrete bricks and tiles were used [7–11]. While using concretes, the prolonged exposure to radiation causes the water content to get absorbed, and consequently, the wall falls off quickly. Following the ordinary concretes, various materials were tested for the shielding purposes like special concretes, polymers, alloys, glasses, etc. [12–19]. On the other hand, glass possesses outstanding features such as high density, durability, rust resistance, moisture resistance, and transparency [20–25], making it an improved replacement for concretes.

Investigations on rare-earth doped oxide glasses have been carried out in recent decades in photonics and radiation physics. Among several oxide glasses, borate and tellurite are the two major host matrices involved in bringing out the best version of the glass material with high chemical and thermal stability, low phonon

* Corresponding author.
E-mail address: mari_ram2000@yahoo.com (K. Marimuthu).

https://doi.org/10.1016/j.net.2022.05.006

maxima, high dielectric constant, and low crystallization ability [24,26]. TeO_2 doping into the alkali borate glasses lessens the latter's hygroscopic behavior and enhances its refractive index, durability, and infrared transmittance [27]. Furthermore, TeO_2 is also called a non-conventional glass former and cannot transform itself into a glassy state on its own [28]. Moreover, a study carried out by Kaur et al. [29] on the potassium tellurite glasses has shown that up to a certain level of K_2O content, the non-bridging oxygens (NonBO) are created, and TeO_4 tetrahedra do not change into TeO_3 groups. And if the K_2O content further increases, TeO_4 transforms into TeO_3 groups. The B_2O_3 is one of the glass formers with a high glass-forming ability at normal quenching rates. Borate glasses have irregular network comprising tetrahedral and trigonal boron, and their blend structures diborate, triborate, tetraborate, and pentaborate units. Boro-tellurite glasses have potential applications, particularly in micro-electronics and Opto-acoustics, attributable to their excellent optical and electrical properties [30–32]. Based on neutron/gamma measurements the crystalline form of α-TeO_2 ($N_{Te\text{-}O} = 4$) consists of only Te^{4+} (tetrahedral coordination) with oxygen, whereas the pure form of TeO_2 has Non-BO < 4. When alkali metals oxides such as Na_2CO_3 and K_2CO_3 (act as glass modifiers) added to oxide glasses the rise in the Non-BO is confirmed in the glass structure which further influences the thermal and optical properties of the glass as well. Among lanthanides, the trivalent europium ion has the non-degeneracy level of the ground state ($^7F_0$) and excited state ($^5D_0$) which provides particulars about the symmetry around the Eu^{3+} ions site and inhomogeneity of the ligand field [33].

Kebaili et al. observed the radiation protecting abilities of lithium boro-tellurite glasses using the Geant4 code technique [34]. Sayyed et al. reported shielding attributes of borosilicate glasses with the addition of varied BaO content [35]. Lakshminarayana et al. analyzed the radiation protection features of the boro-tellurite glasses, and the MCNP5 code was used to estimate the μ/ρ in the range of 0.015–15 MeV [36]. Dogra et al. studied and reported the radiation shielding features of Bi_2O_3–BaO–B_2O_3–Na_2O glasses using ^{137}CS source [37].

The focus of the present work is to shed light on the optical and radiation resisting aptitude of a new series of multicomponent unleaded glasses incorporated with modifiers such as Li, Ca, Ba, Sr, and Zn. The Physical, structural, elastic, and radiation shielding parameters of the prepared glasses were explored to observe the structural changes. The physical and structural traits such as density, the molar volume of the glass, and rare-earth concentration were estimated by the formulae which are reported earlier [36,37]. The optical parameters such as optical bandgap energy (E_g), band tailing parameters (B) and urbach energy (ΔE) were determined through the absorption spectra employing the tauc's plot. The ability of a shielding medium is governed by some of its features like MAC, HVL and mean free path (MFP) which are calculated and discussed for the present samples in this report [38–40]. The results attained would be good for the scientific society to comprehend the potential effect of modifiers on the radiation resisting quality of the unleaded multicomponent glasses.

2. Experimental methods

The glass composition in the present work is $39H_3BO_3$–$25TeO_2$–$15MO$–$10Na_2CO_3$ –$10K_2CO_3$–$1Eu_2O_3$ (M = Li_2O, CaO, BaO, SrO, ZnO) and was manufactured by melt quenching technique. The precursors such as boric acid, tellurium dioxide, potassium carbonate, sodium carbonate, Europium dioxide, and all other modifiers of high purity analytical grade (99.99%) were purchased from Sigma Aldrich. The mixture is heated at 950 °C for 25min; consecutively, the melt is shaken to ensure the mixture's homogeneity, and form bubbles free glasses. The annealing is done for 8 h at 350 °C to improve the mechanical strength and remove the strain in the glasses. The prepared glasses were polished on both sides before going for characterizations.

BTLi:Eu – $39H_3BO_3$+$25TeO_2$+$15Li_2O$+$10Na_2O$+$10K_2O$+$1Eu_2O_3$

BTCa:Eu – $39H_3BO_3$+$25TeO_2$+$15CaO$+$10Na_2O$+$10K_2O$+$1Eu_2O_3$

BTBa:Eu – $39H_3BO_3$+$25TeO_2$+$15BaO$+$10Na_2O$+$10K_2O$+$1Eu_2O_3$

BTSr:Eu – $39H_3BO_3$+$25TeO_2$+$15SrO$+$10Na_2O$+$10K_2O$+$1Eu_2O_3$

BTZn:Eu – $39H_3BO_3$+$25TeO_2$+$15ZnO$+$10Na_2O$+$10K_2O$+$1Eu_2O_3$

For the structural and optical investigations, the prepared glass samples went through different characterizations with the instruments given in Refs. [41–43].

3. Results and discussion

3.1. XRD and FTIR spectra studies

The XRD pattern of the present glasses was recorded in the range of $10° \leq 2\theta \leq 80°$ and the XRD pattern of the BTCa: Eu glass is shown in Fig. 1 as one of a kind. The pattern reveals a broad band that attributes to the absence of crystalline or sharp peaks, and it has no long-range order in the structure, proving the amorphous character.

Fig. S1 signifies the FaTIR spectra of all the investigated glasses. It was explored to identify a range of stretching and bending vibrations of borate and tellurite units in three different regions such as 400–800 cm^{-1}, 800–1500 cm^{-1}, and 3000–3500 cm^{-1}. The stretching vibrations of the tellurium (Te–O) network generally exhibit two different vibrational modes in the regions 600–640 cm^{-1} and 680–700 cm^{-1}. The two vibrations are (i) Te–O vibration in trigonal bipyramid bands [TeO_4] and (ii) Te–O vibration in trigonal pyramid bands [TeO_3] [44]. The broad peaks reveal the mixed form of TeO_3 group, TeO_4 group, and the deformed structure

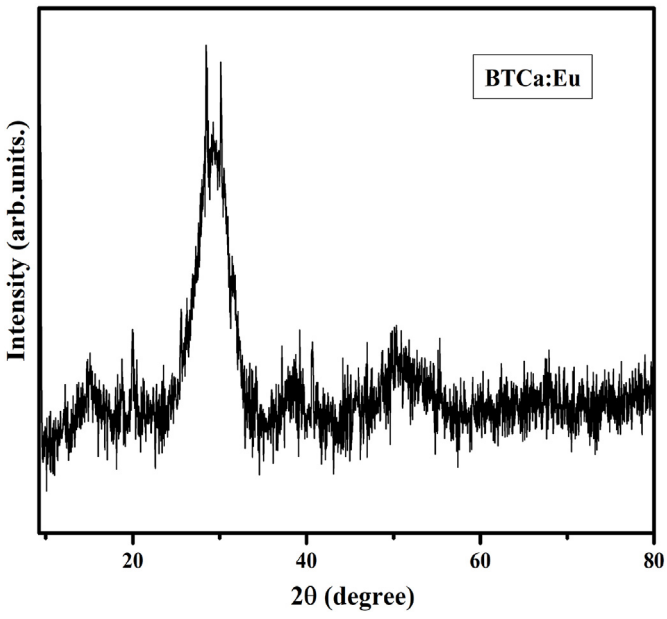

Fig. 1. XRD pattern of BTCa:Eu glass.

of TeO_4 group [45]. Similarly, in the absorbance of borate glasses, the vibrational modes are active in IR spectral region, and the spectral regions were divided into three bands at around 700 cm^{-1}, 800–1200 $cm^{-1,}$ and 1200–1600 cm^{-1}. The band at 700 cm^{-1} is due to the B–O–B bending modes of BO_3 and BO_4 units. The bands in the region 1200–1600 cm^{-1} are due to the B–O bond stretching of BO_4 units and the bands around 1200–1600 cm^{-1} gives the information about the asymmetric stretching vibrations of the B–O bond of BO_3 trigonal units.

The band positions of all the prepared glasses are on par with the reported boro-tellurite glasses [46]. The observed band around 2873–3500 cm^{-1} is due to the fundamental stretching of OH group. The bands at around 1725–1830 cm^{-1} were attributed to the presence of NonBO [33]. The band positioned at around 1241 cm^{-1} is attributed to the stretching vibrations of BO bonds of trigonal BO_3 groups in boroxol rings. The absorption peak at around 1001 cm^{-1} is observed due to the B–O stretching vibrations or asymmetric stretching modes of BO_4 vibrations attached with the NonBO in the borate network [47]. The band observed at 705 cm^{-1} is due to B–O–B linkages. The absorption of around 686 cm^{-1} is observed due to the bending vibrations of TeO_3 units. The band positioned at around 465 cm^{-1} is due to the metal oxide bond and cation vibrations in the glass network [48]. The peak positions and their assignments are listed in Table 1.

3.2. Morphological studies

The SEM analysis for one of the prepared glasses (BTZn:Eu) in Fig. 2 (inset). The micrographs of Eu^{3+} doped Zinc boro-tellurite glass is distinguished by three different magnification scales such as 50 μm, 1 μm, and 5 μm in (a), (b), and (c) respectively. It is clear from the images that there is no formation of pristine particles in the respective sample. This specific trait confirms the amorphous nature of the as-prepared sample. Similarly, the incorporation of elemental analysis confirms the presence of all the elements added into the composition. From the results of EDAX spectrum the total wt % in the prepared glass is (BTZn:Eu) 72.04% partitioned by fused elements such as B, Te, Na. K. Zn, Eu, and O.

3.3. Physical attributes

The density (ρ), molar volume (V_m), and Molar refractivity (R_m) of the glass materials play a crucial role in analyzing the glass network and the structural changes that they have undergone. The structural modification in the vitreous glass structures will be visibly reflected in the ρ value of the glasses, which also rely on the structural coordination number. While inserting modifiers into the host matrix, structural compaction occurs, as observed through the ρ measurement. Some of the assessed physical features of the Eu^{3+} doped multicomponent glasses are given in Table 2. The formation of NonBO in the glass matrix caused some unusual changes in the V_m trend, as offered in Table 2. The oxygen distribution in the glass structure is well known to be explored by the V_m; in other words, V_m depends on the Non-BO of the glass system. The addition of the modifiers expanded the glass structure depending on the bridging oxygens.

Furthermore, the metallization criterion (M) verifies the glass matrices to be insulators since $V_m > R_m$. The computed rare-earth ion concentration is higher for the BTZn:Eu glass. The ionic radii and bond length of TeO_2 are higher when compared to B_2O_3. Hence there exists easy occupation of B_2O_3 onto TeO_2. Fig. S2 demonstrates the correlation among ρ, refractive index, and V_m of the studied glasses.

3.4. Structural features

The boron-boron separation (<d_{B-B}>), and oxygen packing density (OPD) values reveal the structure compactness and the presence of NonBO in the glass system [49,50]. The compactness of the glass structure due to the presence of boric acid in high quantity can be assessed by calculating (d_{B-B}), the average boron-boron separation using the following relation [49].

$$d_{B-B} = \left(\frac{V_m^B}{N_A}\right)^{1/3}$$

where, V_m^B is the boron molar volume or volume of 1 mol of boron in a definite structure, and N_A is the Avogadro number. Table 3 shows the structural properties of the Eu^{3+} doped multi constituent glasses. The <d_{B-B}> value differs for each modifier, and it is revealed that due to the inclusion of the modifiers at higher levels inside the disordered glass structure, the d_{B-B} got shortened. It is highly interrelated to the ionic radii of the boron atom and that of the additives. Fig. S3 shows the affiliation among the V_m, V_o, OPD, and <d_{B-B}> of the present glass series. It is noticed that the OPD declines with a rise in V_m of the glasses. The increase/decrease in the OPD exposes the distinction in the packing nature of the glass structure where the network is open for macromolecular chain reaction with rigid nature. One of the significant parameters in the preparation of glass is the glass transition temperature which impacts the construction of the glasses. The as-quenched glasses follow the course BTBa:Eu > BTLi:Eu > BTSr:Eu > BTCa:Eu > BTZn:Eu with a gradual rise in a rigid structure. Furthermore, glasses with less OPD represent mobility inside the network that requires minimal internal energy. Consequently, glasses with more rigidness possess a more significant number of NonBO.

According to the metallization theory proposed by Dimitrov et al. [51], the M will be smaller if Rm/Vm is larger. The lesser value of M makes the width of the gap between valence and conduction band rise. The appraised M value of the titled glasses lies in the range 0.613–0.692 signifying the suitability of the samples for non-metallic fields. The value of Two-photon absorption (β) depends upon the electronic structure of the materials, and the calculated β value for the present glasses was found in the range of 11.15–12.78 cm/GW.

Table 1
Band positions (in cm^{-1}) and the corresponding peak assignments of FTIR spectra of the BTM:Eu glasses.

S.No.	BTLi:Eu	BTCa:Eu	BTSr:Eu	BTBa:Eu	BTZn:Eu	Assignments
1	3012	3014	3102	3020	3109	O-H stretching vibrations
2	2923	2910	2941	2935	2932	Hydrogen Bonding
3	2848	2851	2811	2857	2546	Hydrogen Bonding
4	1001	1012	-	1016	1015	B-O stretching vibrations of BO_3
5	704	705	705	706	705	Vibration of B-O-B linkages
6	611	615	611	611	618	Symmetric stretching vibrations of Te-O in TeO_4
7	693	699	686	686	672	Bending vibrations in TeO_3
8	-	-	-	-	435	Stretching and bending vibrations of ZnO bond

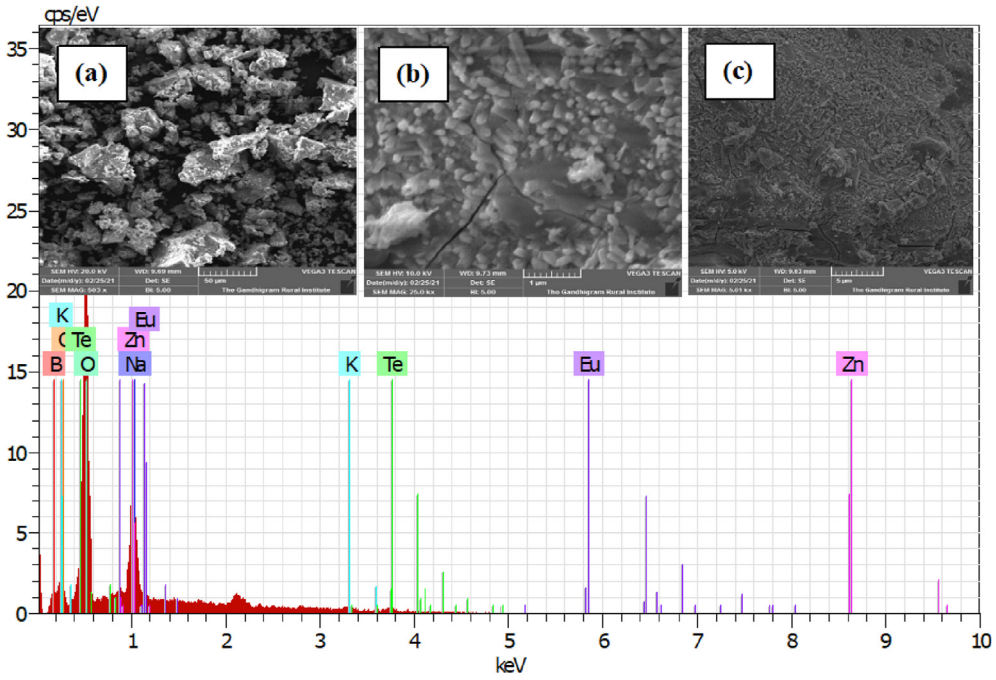

Fig. 2. The elements occupied in the prepared glass were titled for BTZn:Eu glass. Their respective morphological analysis was shown in the inset as (a) 50 μm (b) 1 μm (c) 5 μm respectively.

Table 2
Physical properties of BTM:Eu glasses.

Physical Properties	BTLi:Eu	BTCa:Eu	BTSr:Eu	BTBa:Eu	BTZn:Eu
Density (ρ, g/cm^3)	3.149	3.546	3.589	3.601	3.898
Refractive index (n)	1.517	1.524	1.552	1.580	1.677
Average molecular weight (M, g)	103.03	106.96	114.09	104.16	121.55
Molar volume (V_m, cm^3/mol)	32.71	33.65	31.78	30.15	26.78
Molar refractivity (R_m, cm^3)	9.296	9.826	10.157	11.200	10.063
Metallization criterion (M)	0.691	0.692	0.672	0.661	0.613
Rare Earth ion concentration (N, × 10^{20} ions/cm^3)	3.681	3.994	3.788	3.577	4.507

Table 3
Structural properties of the BTM:Eu glasses.

Structural properties	BTLi:Eu	BTCa:Eu	BTSr:Eu	BTBa:Eu	BTZn:Eu
Boron-Boron separation (d_{B-B} × 10^{-10}m)	3.82	3.79	3.93	3.85	3.57
Oxygen molar volume (V_o, cm^3/mol)	11.45	10.59	12.19	11.78	9.35
Oxygen packing density (OPD, mol/cm^3)	84.06	91.19	86.51	81.51	91.68
Nearest neighbor coordination number (n_{av})	4.36	4.27	4.00	4.36	4.36
Optical basicity (Λ_{th})	1.0634	1.0067	1.0421	1.068	1.0039
Two photon absorption (β)	11.15	12.78	12.62	12.39	12.54
Bond density (n_b, × 10^{28}m^{-3})	8.04	8.53	7.59	7.80	9.84
Ionic factor (I_c, %)	91.33	96.62	96.82	97.05	93.27
Covalency factor (C_c, %)	8.67	3.38	3.18	2.95	6.73

The nearest neighbor coordination number opposes the boron-boron separation values for the investigated glasses. The nearest neighbor coordination number and bond density increase reduce the d_{B-B} values [52]. Another crucial parameter of glass is basicity, which governs the electron donating power of an oxygen atom in an oxide glass network. In Table 3, the structural properties of the Eu^{3+} ions doped glasses are submitted. The OPD and basicity values show the same course following the modifier in the glass composition. The structural deviations can also be examined by analyzing the ionic or covalent character of the glasses established in terms of the electronegativity difference between the anion and cation [53]. It is observed from Table 3 that the ionic factor ranges from 91.33 to 97.05%, whereas the covalent factor ranges from 2.95 to 8.67%. The ionicity is maximum for all the glasses irrespective of different modifiers in the composition, which proves that the prepared glasses are ionic.

3.5. Mechanical attributes

The elastic moduli are estimated for the present Eu^{3+} doped multi-component glasses and listed in Table 4. The young's and bulk modulus values of the samples follow the trend

Table 4
Elastic properties of the BTM:Eu glasses.

Elastic properties	BTLi:Eu	BTCa:Eu	BTSr:Eu	BTBa:Eu	BTZn:Eu
Young's modulus (E, Gpa)	83.12	75.15	65.76	63.72	79.92
Bulk modulus (K, Gpa)	58.80	50.18	39.88	38.97	52.11
Shear modulus (G, Gpa)	32.84	30.05	26.80	26.02	32.12
Poisson's ratio (σ)	0.26	0.25	0.22	0.22	0.24
Fractal bond connectivity (d)	2.23	2.39	2.68	2.67	2.46
Hardness (H, Gpa)	5.15	5.00	4.91	4.72	5.47

BTLi:Eu > BTZn:Eu > BTCa:Eu > BTSr:Eu > BTBa:Eu. The Poisson's ratio follows a different trend BTLi:Eu > BTZn:Eu > BTCa:Eu > BTSr:Eu = BTBa:Eu for the studied glasses. Among all the glasses, the BTLi:Eu glass is more compact and rigid which is highly required for shielding radiations. Usually, when the Poisson's value falls in the range 0.1–0.2, then the connectivity of the glass is perceived to be high. The present work's values lie in the range 0.22–0.26, thus claiming better connectivity in the glass structure. The fractal bond connectivity (d) results lie in the range 2.23–2.68, which indicates the 2D structure of the prepared glass matrices. The hardness (H) of the glass explicitly indicates the amount of stress required to neglect the free volume in glass [52]. For the studied glasses, H falls in the range 4.72–5.47 GPa, implying the hardness and resistance of the glasses to be penetrated, and it is high for BTZn:Eu glass.

3.6. Optical analysis and band gap estimation

Fig. 3 reveals the optical absorption spectrum of the BTBa:Eu glass recorded in the range 350–2300 nm. The observed absorption bands arise due to the f–f optical excitation from the ground state ($^7F_0$ and $^7F_1$) to various excited states and the bands centered at around 390, 475, 520, 720, 2090, and 2207 nm correspond to the transitions $^7F_0 \rightarrow {}^5D_2$, $^7F_0 \rightarrow {}^5D_1$, $^7F_1 \rightarrow {}^5D_1$, $^7F_0 \rightarrow {}^5D_0$, $^7F_0 \rightarrow {}^7F_6$ and $^7F_1 \rightarrow {}^7F_6$ respectively [54]. The parameters such as Nephelauxetic ratio ($\overline{\beta}$) and bonding parameter (δ) are used to examine the bonding nature of the glass samples [55]. Using the aquo ion [56] as a reference, the parameters are computed and presented in Table S1. Following the ligand field, δ will come out as positive or negative, representing the covalent or ionic nature of the bond. The nature of the bond in the prepared Eu^{3+} doped multi constituent glasses is revealed to be covalent from the evaluated positive δ values and the covalent nature rises in the order BTZn:Eu > BTBa:Eu > BTLi:Eu > BTCa:Eu > BTSr:Eu.

The band gap energy (E_g) values of the glassy materials assessed from the optical absorption spectra offer detailed information about the optically induced transitions. For pure crystalline components owning sharp conduction and valence band edges, the energy bands will be precisely defined. On the other side, the glassy constituents display the tailing of the localized states into the forbidden energy gap. Using the optical absorption spectra, the tauc's plot for direct and indirect E_g of the prepared glass samples are plotted and shown in Fig. 4 (a) and (b), respectively [57]. The directly deduced E_g values are found to be 3.29, 3.34, 3.39, 3.20, 3.36 (direct E_g eV) and 3.82, 3.82, 3.84, 3.80, 3.83 (indirect E_g eV) for the BTBa:Eu, BTSr:Eu, BTLi:Eu, BTCa:Eu, BTZn:Eu glasses respectively. The BTBa:Eu is noticed to hold higher E_g value, proposing a better shielding channel to resist harmful radiations. The rise in the E_g accounts for the decrease in the non-bridging oxygens due to the rise in the oxygen anions in the glass structure.

The measure of imperfections in the glass is preferably attained using Urbach energy (ΔE) values in the range of 0.10–0.87eV for the investigated glass set. Table S1 shows the optical band gap and Urbach's energy values of the synthesized glasses. The reduction in the ΔE values depicts the stability and homogeneity of the samples due to the reduction in the defects and disorders in the glass matrices [41].

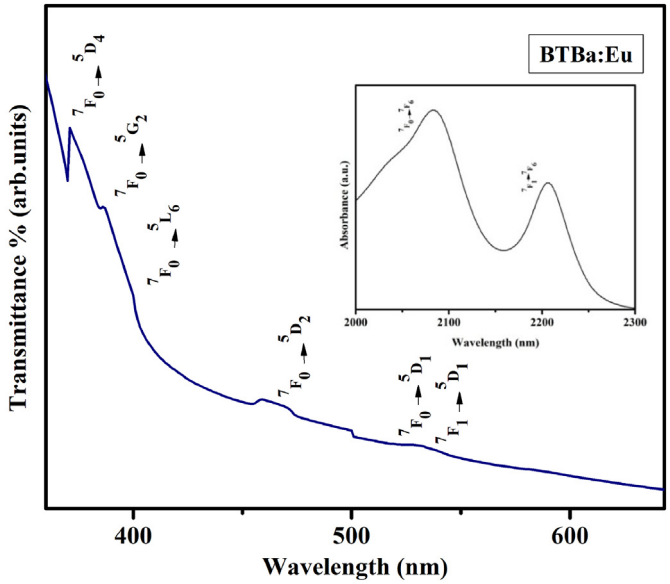

Fig. 3. Absorption spectrum of BTBa:Eu glass.

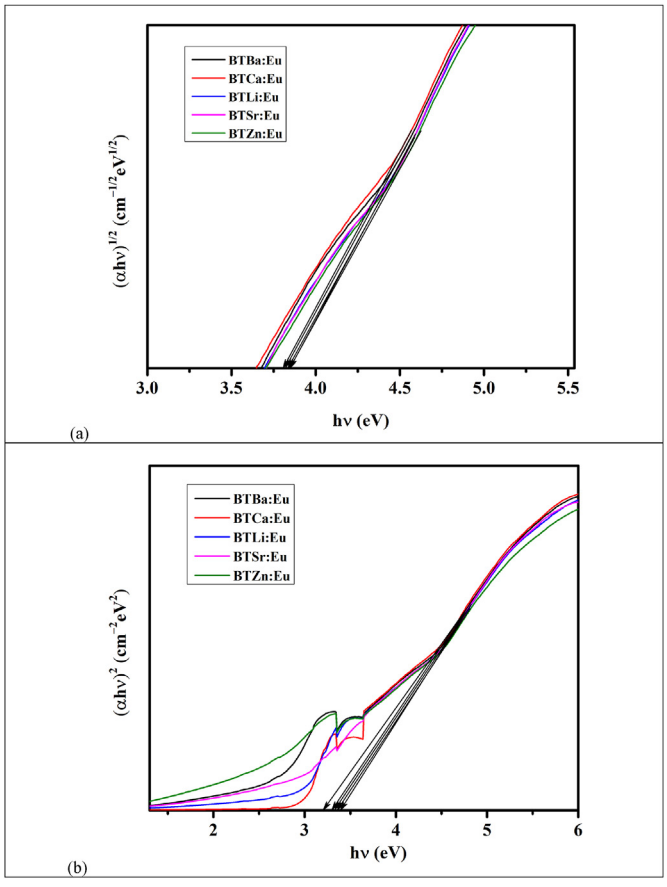

Fig. 4. **(a)** Tauc's plot for direct transitions (n = 1/2) of the BTM:Eu glasses. **(b)** Tauc's plot for Indirect transitions (n = 2) of the BTM:Eu glasses.

3.7. Radiation shielding features

We investigated the radiation attenuation attributes of the prepared Eu^{3+} ions doped multi constituent glasses using Phy-X software [58]. We investigated the radiation attenuation factors for the energy range varied between 0.284 and 1.33 MeV. We determined the linear attenuation coefficient (LAC) and examined the influence of the five oxides Li_2O_3, CaO, BaO, SrO, and ZnO on the LAC values (see Fig. 5). The LAC decreases exponentially as the energy increases, and this finding follows the Lambert-Beer law (i.e. $I=I_0 \exp^{-LAC*x}$). This implies that the glasses with different oxides have good attenuation performance at low energy and the LAC varied between 0.433 and 0.549 cm^{-1} at the first low energy used in this work. When the energy increases to the second energy in this work (i.e., 0.347 MeV), the LAC becomes in the order of 0.362–0.448 cm^{-1}. One must remember that the photoelectric effect is an important process at such low energies, so the LAC has high values for all glasses regardless of the type of oxide used. The LAC is still in decreasing trend, and the lowest values happened at 1.33 MeV and are equal to 0.163, 0.184, 0.184, 0.185, and 0.202 cm^{-1} for BTLi:Eu, BTCa:Eu, BTBa:Eu, BTSr:Eu and BTZn:Eu. If we consider one specific energy, we can investigate the influence of the five oxides on the LAC values. The BTLi:Eu glass has a much smaller LAC than the other glasses, and this is expected since the atomic number of Li is small and it has a feeble attenuation ability against gamma radiation. Also, the density of BTLi:Eu is smaller than the rest of the glasses, so it has the least LAC. While the density of BTZn:Eu is higher than the other glasses, and has the highest LAC.

From the LAC, we examined the HVL. The importance of this parameter is that it gives information about the thickness of the layer that can attenuate 50% of the radiation. In Fig. 6, we investigated the influence of the energy and the different oxides used in the glasses on the HVL. The first observation from this figure is the relation between the energy and the HVL. The HVL for the glasses with different compositions is less than 1.5 cm at 0.284 MeV, and this is the smallest HVL observed for these samples. This reflects the importance of using a thin layer of these glasses to shield the photons with low energy. Increasing the energy means that we need a sample with a higher thickness to shield the photons, and this thickness is less than 2 cm at 0.347 MeV and varies between 2 and -2.5 cm at 0.511 MeV. At 1.33 MeV, the thickness of the samples needed to attenuate the photons becomes 3.4–4.2 cm, so a thick glass is recommended to be utilized in high-energy applications

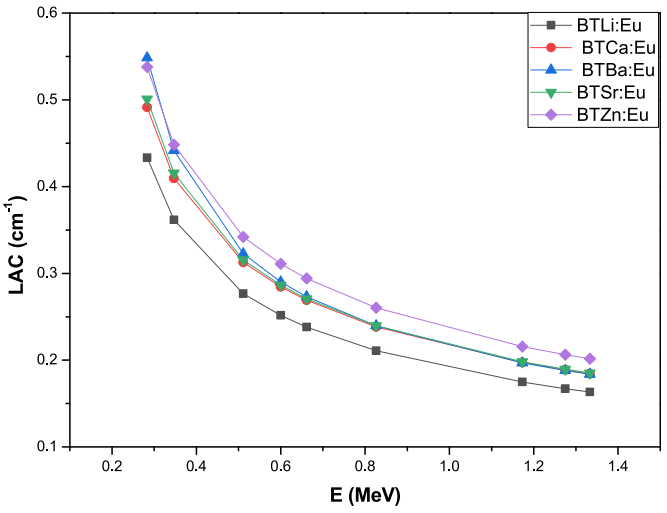

Fig. 5. The linear attenuation coefficient for the BTM:Eu glasses.

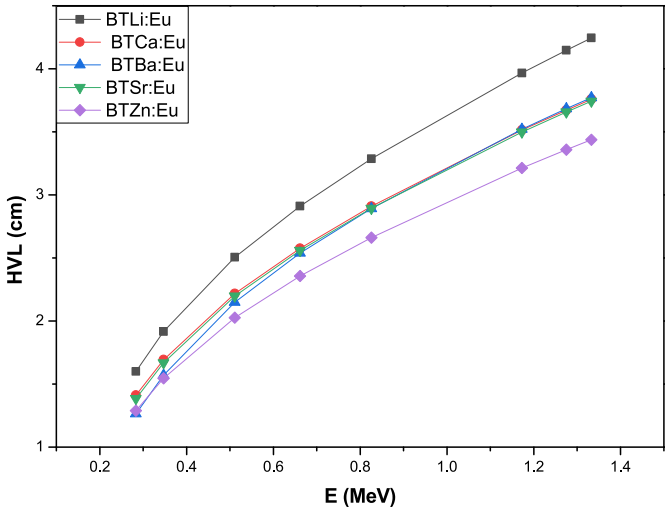

Fig. 6. The half value layer (HVL) for the BTM:Eu glasses.

(less than 1.5 MeV). The second observation from Fig. 6, the relation between the HVL and the type of oxides used in the glasses. If we look at the HVL for the sample with Li_2O_3, we see that the HVL of this composition is higher than the other compositions. While, due to the high density of BTZn:Eu sample, it has the least HVL.

We compared the tenth value layer (TVL) for our prepared Eu^{3+} ions doped multi constituent glasses with other glass systems at 0.662 MeV. In Fig. 7, we compared the TVL for these glasses with the BaO−-Li_2O-B_2O_3glass system [4]. Clearly, due to the low density of BTLi:Eu, it has higher TVL than the BaO-Li_2O-B_2O_3 glasses with different compositions. BTZn:Eu has a very close TVL with 25BaO-15Li_2O-60B_2O_3 glass. BTCa:Eu, BTBa:Eu, and BTSr:Eu have lower TVL than 35BaO-5Li_2O-60B_2O_3, but higher TVL than 30BaO10-Li_2O−60B_2O_3. In Fig. S4, we compared the investigated glasses in this study with the CaF_2-BaO−P_2O_5 glass system [3]. Again, BTLi:Eu has higher TVL than all the selected CaF_2−BaO−P_2O_5glasses. Due to the relatively high density of BTZn:Eu, it has lower TVL than all the CaF_2−BaO−P_2O_5glasses. BTBa:Eu has almost the same TVL with the 6CaF_2−44BaO−50P_2O_5 sample, while BTCa:Eu has a very close TVL with 4CaF_2−46BaO−P_2O_5.

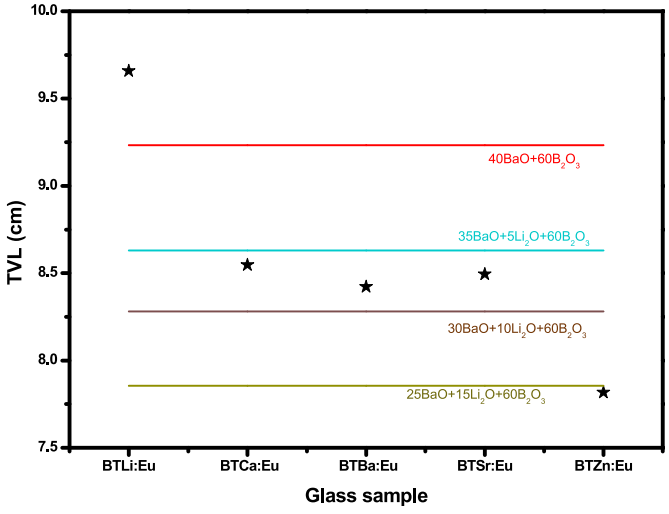

Fig. 7. Comparison between the tenth value layers for the prepared BTM:Eu glasses and BaO-Li_2O-B_2O_3 glass system at 0.662 MeV.

4. Conclusion

In this work, the compositional dependent Eu^{3+} doped multi constituent glasses are prepared and analyzed through XRD, FTIR, and other techniques. The amorphous structure of the glasses was revealed via the XRD measurement. FTIR analysis validated the stretching and bending vibrations of BO_3/BO_4, and TeO_4/TeO_3 functional groups in the titled glasses. The density and refractive index of the prepared glasses were calculated to vary almost linearly depending on the incorporated modifiers. Investigation of the structural properties like OPD and V_O confirms the presence of a higher amount of bridging oxygen sites, making the glass matrix tightly packed. The evaluation of β evidenced the prepared glasses as effective source materials for any nonlinear or photonic applications. The computed elastic moduli expose the BTLi:Eu glass to be tightly packed and rigid, required for a superior shielding channel. The higher bandgap values for BTLi:Eu glass and the calculated Urbach's energy value reveals that the prepared glasses own lesser defects essential for better shielding. The radiation shielding performance was investigated in LAC, HVL, and MFP. At 0.347 MeV, the MFP follows the order BTLi:Eu > BTCa:Eu > BTSr:Eu > BTBa:Eu > BTZn:Eu. The BTLi:Eu, glass has a higher TVL than the BaO Li_2O–B_2O_3 glass system. BTZn:Eu has very close TVL with $25BaO–15Li_2O–60B_2O_3$ glass. BTCa:Eu, BTBa:Eu and BTSr:Eu have lower TVL than $35BaO–5Li_2O–60B_2O_3$.

Declaration of competing interest

The authors declare that they have no known competing financial interests or personal relationships that could have appeared to influence the work reported in this paper.

Acknowledgment

The authors express their gratitude to Princess Nourah bint Abdulrahman University Researchers Supporting Project Number (PNURSP2022R111), princess Nourah bint Abdulrahman University, Riyadh, Saudi Arabia.

Appendix A. Supplementary data

Supplementary data to this article can be found online at https://doi.org/10.1016/j.net.2022.05.006.

References

[1] Mengge Dong, Suying Zhou, Xiangxin Xue, M.I. Sayyed, Daria Tishkevich, Alex Trukhanov, Chao Wang, Study of comprehensive shielding behaviors of chambersite deposit for neutron and gamma ray, Prog. Nucl. Energy 146 (2022), 104155, https://doi.org/10.1016/j.pnucene.2022.104155.

[2] I.O. Olarinoye, S. Alomairy, C. Sriwunkum, M.S. Al-Buriahi, Effect of Ag_2O/V_2O_5 substitution on the radiation shielding ability of tellurite glass system via XCOM approach and FLUKA simulations, Phys. Scripta 96 (2021), 065308, https://doi.org/10.1088/1402-4896/abf26a.

[3] Y. Al-Hadeethi, M.I. Sayyed, Evaluation of gamma ray shielding characteristics of $CaF_2–BaO–P_2O_5$ glass system using Phy-X/PSD computer program, Prog. Nucl. Energy 126 (2020), 103397, https://doi.org/10.1016/j.pnucene.2020.103397.

[4] Y. Al-Hadeethi, M.I. Sayyed, $BaO–Li_2O–B_2O_3$ glass systems: potential utilization in gamma radiation protection, Prog. Nucl. Energy 129 (2020), 103511, https://doi.org/10.1016/j.pnucene.2020.103511.

[5] M. Kamislioglu, Research on the effects of bismuth borate glass system on nuclear radiation shielding parameters, Results Phys. 22 (2021) 103844, https://doi.org/10.1016/j.rinp.2021.103844.

[6] B.O. Elbashir, M.G. Dong, M.I Sayyed, S.A.M. Issa, K.A. Matori, M.H.M. Zaid, Comparison of Monte Carlo simulation of gamma ray attenuation coefficients of amino acids with XCOM program and experimental data, Results Phys. 9 (2018) 6–11, https://doi.org/10.1016/j.rinp.2018.01.075.

[7] N.K. Libeesh, K.A. Naseer, K.A. Mahmoud, M.I. Sayyed, S. Arivazhagan, M.S. Alqahtani, E.S. Yousef, M.U. Khandaker, Applicability of the multispectral remote sensing on determining the natural rock complexes distribution and their evaluability on the radiation protection applications, Radiat. Phys. Chem. 193 (2022), 110004, https://doi.org/10.1016/j.radphyschem.2022.110004.

[8] N.K. Libeesh, K.A. Naseer, S. Arivazhagan, A.F. Abd El-Rehim, K.A. Mahmoud, M.I. Sayyed, M.U. Khandaker, Advanced nuclear radiation shielding studies of some mafic and ultramafic complexes with lithological mapping, Radiat. Phys. Chem. 189 (2021), 109777, https://doi.org/10.1016/j.radphyschem.2021.109777.

[9] N.K. Libeesh, K.A. Naseer, S. Arivazhagan, A.F.A. El-Rehim, G. ALMisned, H.O. Tekin, Characterization of Ultramafic–Alkaline–Carbonatite complex for radiation shielding competencies: an experimental and Monte Carlo study with lithological mapping, Ore Geol. Rev. 142 (2022), 104735, https://doi.org/10.1016/j.oregeorev.2022.104735.

[10] N.K. Libeesh, K.A. Naseer, S. Arivazhagan, K.A. Mahmoud, M.I. Sayyed, M.S. Alqahtani, E.S. Yousef, Multispectral remote sensing for determination the Ultra-mafic complexes distribution and their applications in reducing the equivalent dose from the radioactive wastes, Eur. Phys. J. Plus. 137 (2022) 267, https://doi.org/10.1140/epjp/s13360-022-02473-5.

[11] S. Arivazhagan, K.A. Naseer, K.A. Mahmoud, K.V. Arun Kumar, N.K. Libeesh, M.I. Sayyed, M.S. Alqahtani, E.S. Yousef, M.U. Khandaker, Gamma-ray protection capacity evaluation and satellite data based mapping for the limestone, charnockite, and gneiss rocks in the Sirugudi taluk of the Dindigul district, India, Radiat, Phys. Chem. 196 (2022), 110108, https://doi.org/10.1016/j.radphyschem.2022.110108.

[12] O. Agar, M.I. Sayyed, H.O. Tekin, K.M. Kaky, S.O. Baki, I. Kityk, An investigation on shielding properties of BaO, MoO3 and P2O5 based glasses using MCNPX code, Results Phys. 12 (2019) 629–634, 109386, https://doi.org/10.1016/j.rinp.2018.12.003.

[13] A. Saeed, S. Alomairy, C. Sriwunkum, M.S. Al-Buriahi, Neutron and charged particle attenuation properties of volcanic rocks, Radiat. Phys. Chem. 184 (2021), 109454, https://doi.org/10.1016/j.radphyschem.2021.109454.

[14] M.S. Al-Buriahi, S. Alomairy, C. Mutuwong, Effects of MgO addition on the radiation attenuation properties of 45S5 bioglass system at the energies of medical interest: an in silico study, J. Australas. Ceram. Soc. 57 (2021) 1107–1115, https://doi.org/10.1007/s41779-021-00605-1.

[15] G. Kilic, E. Ilik, S.A.M. Issa, H.O.O. Tekin, Synthesis and structural, optical, physical properties of Gadolinium (III) oxide reinforced $TeO_2–B_2O_3–(20\text{-}x)Li_2O\text{-}xGd_2O_3$ glass system, J. Alloys Compd. 877 (2021), 160302, https://doi.org/10.1016/j.jallcom.2021.160302.

[16] M.S. Al-Buriahi, C. Eke, S. Alomairy, A. Yildirim, H.I. Alsaeedy, C. Sriwunkum, Radiation attenuation properties of some commercial polymers for advanced shielding applications at low energies, Polym. Adv. Technol. 32 (2021) 2386–2396, https://doi.org/10.1002/pat.5267.

[17] G. Kilic, E. Ilik, S.A.M. Issa, B. Issa, U.G. Issever, H.M.H. Zakaly, H.O. Tekin, Fabrication, structural, optical, physical and radiation shielding characterization of indium (III) oxide reinforced $85TeO_2\text{-}(15–x)ZnO\text{-}xIn_2O_3$ glass system, Ceram. Int. 47 (2021) 27305–27315, https://doi.org/10.1016/j.ceramint.2021.06.152.

[18] G. Kilic, E. Ilik, S.A.M. Issa, B. Issa, M.S. Al-Buriahi, U.G. Issever, H.M.H. Zakaly, H.O. Tekin, Ytterbium (III) oxide reinforced novel $TeO_2–B_2O_3–V_2O_5$ glass system: synthesis and optical, structural, physical and thermal properties, Ceram. Int. 47 (2021) 18517–18531, https://doi.org/10.1016/j.ceramint.2021.03.175.

[19] G. Kilic, E. Ilik, K.A. Mahmoud, F.I. El-Agawany, S. Alomairy, Y.S. Rammah, The role of B_2O_3 on the structural, thermal, and radiation protection efficacy of vanadium phosphate glasses, Appl. Phys. A 127 (2021) 265, https://doi.org/10.1007/s00339-021-04409-9.

[20] K.A. Naseer, K. Marimuthu, M.S. Al-Buriahi, A. Alalawi, H.O. Tekin, Influence of Bi_2O_3 concentration on barium-telluro-borate glasses: physical, structural and radiation-shielding properties, Ceram. Int. 47 (2021) 329–340, https://doi.org/10.1016/j.ceramint.2020.08.138.

[21] M.S. Al-Buriahi, Y.S.M. Alajerami, A.S. Abouhaswa, A. Alalawi, T. Nutaro, B. Tonguc, Effect of chromium oxide on the physical, optical, and radiation shielding properties of lead sodium borate glasses, J. Non-Cryst. Solids 544 (2020), 120171, https://doi.org/10.1016/j.jnoncrysol.2020.120171.

[22] A.S. Abouhaswa, M.S. Al-Buriahi, M. Chalermpon, Y.S. Rammah, Influence of ZrO_2 on gamma shielding properties of lead borate glasses, Appl. Phys. A 126 (2020) 78, https://doi.org/10.1007/s00339-019-3264-7.

[23] J.S. Alzahrani, M.A. Alothman, C. Eke, H. Al-Ghamdi, D.A. Aloraini, M.S. Al-Buriahi, Simulating the radiation shielding properties of $TeO_2–Na_2O–TiO$ glass system using PHITS Monte Carlo code, Comput. Mater. Sci. 196 (2021), 110566, https://doi.org/10.1016/j.commatsci.2021.110566.

[24] G. Kilic, S.A.M. Issa, E. Ilik, O. Kilicoglu, U.G. Issever, R. El-Mallawany, B. Issa, H.O. Tekin, Physical, thermal, optical, structural and nuclear radiation shielding properties of Sm_2O_3 reinforced borotellurite glasses, Ceram. Int. 47 (2021) 6154–6168, https://doi.org/10.1016/j.ceramint.2020.10.194.

[25] G.A. Alharshan, C. Eke, M.S. Al-Buriahi, Radiation-transmission and self-absorption factors of $P_2O_5 – SrO – Sb_2O_3$ glass system, Radiat, Phys. Chem. 193 (2022), 109938, https://doi.org/10.1016/j.radphyschem.2021.109938.

[26] G. Kilic, F.I.E.I.E. Agawany, B.O. Ilik, K.A.A. Mahmoud, E. Ilik, Y.S.S. Rammah, Ta_2O_5 reinforced $Bi_2O_3–TeO_2–ZnO$ glasses: fabrication, physical, structural characterization, and radiation shielding efficacy, Opt. Mater. 112 (2021), 110757, https://doi.org/10.1016/j.optmat.2020.110757.

[27] M.I. Sayyed, N. Dwaikat, M.H.A. Mhareb, A.N. D'Souza, N. Almousa, Y.S.M. Alajerami, F. Almasoud, K.A. Naseer, S.D. Kamath, M.U. Khandaker,

H. Osman, S. Alamri, Effect of TeO_2 addition on the gamma radiation shielding competence and mechanical properties of boro-tellurite glass: an experimental approach, J. Mater. Res. Technol. 18 (2022) 1017–1027, https://doi.org/10.1016/j.jmrt.2022.02.130.
[28] P. Vani, G. Vinitha, K.A. Naseer, K. Marimuthu, M. Durairaj, T.C. Sabari Girisun, N. Manikandan, Thulium-doped barium tellurite glasses: structural, thermal, linear, and non-linear optical investigations, J. Mater. Sci. Mater. Electron. 32 (2021) 23030–23046, https://doi.org/10.1007/s10854-021-06787-5.
[29] N. Kaur, A. Khanna, Structural characterization of borotellurite and alumino-borotellurite glasses, J. Non-Cryst. Solids 404 (2014) 116–123, https://doi.org/10.1016/j.jnoncrysol.2014.08.002.
[30] Z.A. Said Mahraz, M.R. Sahar, S.K. Ghoshal, M. Reza Dousti, Concentration dependent luminescence quenching of Er^{3+}-doped zinc boro-tellurite glass, J. Lumin. 144 (2013) 139–145, https://doi.org/10.1016/j.jlumin.2013.06.050.
[31] K.A. Naseer, P. Karthikeyan, S. Arunkumar, P. Suthanthirakumar, K. Marimuthu, Enhanced luminescence properties of Er^{3+}/Yb^{3+} doped zinc tellurofluoroborate glasses for 1.5 μm optical amplification, in: AIP Conf. Proc., AIP Conference Proceedings, 2020, https://doi.org/10.1063/5.0019171, 030237.
[32] K.A. Naseer, K. Marimuthu, The impact of Er/Yb co-doping on the spectroscopic performance of bismuth borophosphate glasses for photonic applications, Vacuum 183 (2021), 109788, https://doi.org/10.1016/j.vacuum.2020.109788.
[33] K. Annapoorani, K. Marimuthu, Spectroscopic properties of Eu^{3+} ions doped Barium telluroborate glasses for red laser applications, J. Non-Cryst. Solids 463 (2017) 148–157, https://doi.org/10.1016/j.jnoncrysol.2017.03.004.
[34] I. Kebaili, M.I. Sayyed, I. Boukhris, M.S. Al-Buriahi, Gamma-ray shielding parameters of lithium borotellurite glasses using Geant4 code, Appl. Phys. A 126 (2020) 536, https://doi.org/10.1007/s00339-020-03702-3.
[35] M.I. Sayyed, G. Lakshminarayana, Structural, thermal, optical features and shielding parameters investigations of optical glasses for gamma radiation shielding and defense applications, J. Non-Cryst. Solids 487 (2018) 53–59, https://doi.org/10.1016/j.jnoncrysol.2018.02.014.
[36] G. Lakshminarayana, S.O. Baki, A. Lira, I.V. Kityk, M.A. Mahdi, Structural, thermal, and optical absorption studies of Er^{3+}, Tm^{3+}, and Pr^{3+}-doped borotellurite glasses, J. Non-Cryst. Solids 459 (2017) 150–159, https://doi.org/10.1016/j.jnoncrysol.2017.01.006.
[37] M. Dogra, K.J. Singh, K. Kaur, V. Anand, P. Kaur, P. Singh, B.S. Bajwa, Investigation of gamma ray shielding, structural and dissolution rate properties of Bi_2O_3 -BaO-B_2O_3 -Na_2O glass system, Radiat, Phys. Chem. 144 (2018) 171–179, https://doi.org/10.1016/j.radphyschem.2017.08.008.
[38] B.T. Tonguc, H. Arslan, M.S. Al-Buriahi, Studies on mass attenuation coefficients, effective atomic numbers and electron densities for some biomolecules, Radiat. Phys. Chem. 153 (2018) 86–91, https://doi.org/10.1016/j.radphyschem.2018.08.025.
[39] M.S. Al-Buriahi, B.T. Tonguc, Mass attenuation coefficients, effective atomic numbers and electron densities of some contrast agents for computed tomography, Radiat. Phys. Chem. 166 (2020), 108507, https://doi.org/10.1016/j.radphyschem.2019.108507.
[40] M.S. Al-Buriahi, C. Eke, S. Alomairy, C. Mutuwong, N. Sfina, Micro-hardness and gamma-ray attenuation properties of lead iron phosphate glasses, J. Mater. Sci. Mater. Electron. 32 (2021) 13906–13916, https://doi.org/10.1007/s10854-021-05966-8.
[41] P. Evangelin Teresa, K.A. Naseer, K. Marimuthu, H. Alavian, M.I. Sayyed, Influence of modifiers on the physical, structural, elastic and radiation shielding competence of Dy^{3+} ions doped Alkali boro-tellurite glasses, Radiat. Phys. Chem. 189 (2021), 109741, https://doi.org/10.1016/j.radphyschem.2021.109741.
[42] P.E. Teresa, K.A. Naseer, T. Piotrowski, K. Marimuthu, D.A. Aloraini, A.H. Almuqrin, M.I. Sayyed, Optical properties and radiation shielding studies of europium doped modifier reliant multi former glasses, Optik 247 (2021), 168005, https://doi.org/10.1016/j.ijleo.2021.168005.
[43] P.E. Teresa, R. Divina, K.A. Naseer, K. Marimuthu, Study on the luminescence behavior of Dy^{3+} ions activated, modifier dependent alkali boro-tellurite glasses for white LED application, Optik 259 (2022), 169024, https://doi.org/10.1016/j.ijleo.2022.169024.
[44] P. Karthikeyan, R. Vijayakumar, K. Marimuthu, Luminescence studies on Dy^{3+} doped calcium boro-tellurite glasses for White light applications, Phys. B Condens. Matter 521 (2017) 347–354, https://doi.org/10.1016/j.physb.2017.07.018.
[45] M.N. Ami Hazlin, M.K. Halimah, F.D. Muhammad, M.F. Faznny, Optical properties of zinc borotellurite glass doped with trivalent dysprosium ion, Phys. B Condens. Matter 510 (2017) 38–42, https://doi.org/10.1016/j.physb.2017.01.012.
[46] S. Rada, P. Pascuta, M. Culea, V. Maties, M. Rada, M. Barlea, E. Culea, The local structure of europium–lead-borate glass ceramics, J. Mol. Struct. 924–926 (2009) 89–92, https://doi.org/10.1016/j.molstruc.2008.12.032.
[47] K.A. Naseer, K. Marimuthu, K.A. Mahmoud, M.I. Sayyed, Impact of Bi_2O_3 modifier concentration on barium–zincborate glasses: physical, structural, elastic, and radiation-shielding properties, Eur. Phys. J. Plus. 136 (2021) 116, https://doi.org/10.1140/epjp/s13360-020-01056-6.
[48] P. Suthanthirakumar, C. Basavapoornima, K. Marimuthu, Effect of Pr^{3+} ions concentration on the spectroscopic properties of Zinc telluro-fluoroborate glasses for laser and optical amplifier applications, J. Lumin. 187 (2017) 392–402, https://doi.org/10.1016/j.jlumin.2017.03.052.
[49] G. Sathiyapriya, K.A. Naseer, K. Marimuthu, E. Kavaz, A. Alalawi, M.S. Al-Buriahi, Structural, optical and nuclear radiation shielding properties of strontium barium borate glasses doped with dysprosium and niobium, J. Mater. Sci. Mater. Electron. 32 (2021) 8570–8592, https://doi.org/10.1007/s10854-021-05499-0.
[50] K.A. Naseer, K. Marimuthu, K.A. Mahmoud, M.I. Sayyed, The concentration impact of Yb^{3+} on the bismuth boro-phosphate glasses: physical, structural, optical, elastic, and radiation-shielding properties, Radiat. Phys. Chem. 188 (2021), 109617, https://doi.org/10.1016/j.radphyschem.2021.109617.
[51] V. Dimitrov, S. Sakka, Linear and nonlinear optical properties of simple oxides. II, J. Appl. Phys. 79 (1996) 1741–1745, https://doi.org/10.1063/1.360963.
[52] R. Reddy, Y. Nazeer Ahammed, K. Rama Gopal, D. Raghuram, Optical electronegativity and refractive index of materials, Opt. Mater. 10 (1998) 95–100, https://doi.org/10.1016/S0925-3467(97)00171-7.
[53] M. Kumar, T.K. Seshagiri, M. Mohapatra, V. Natarajan, S.V. Godbole, Synthesis, characterization and studies of radiative properties on Eu^{3+}-doped $ZnAl_2O_4$, J. Lumin. 132 (2012) 2810–2816, https://doi.org/10.1016/j.jlumin.2012.04.033.
[54] S. Pravinraj, M. Vijayakumar, K. Marimuthu, Enhanced luminescence behaviour of Eu^{3+} doped heavy metal oxide telluroborate glasses for Laser and LED applications, Phys. B Condens. Matter 509 (2017) 84–93, https://doi.org/10.1016/j.physb.2017.01.008.
[55] K.A. Naseer, G. Sathiyapriya, K. Marimuthu, T. Piotrowski, M.S. Alqahtani, E.S. Yousef, Optical, elastic, and neutron shielding studies of Nb_2O_5 varied Dy^{3+} doped barium-borate glasses, Optik 251 (2022), 168436, https://doi.org/10.1016/j.ijleo.2021.168436.
[56] W.T. Carnall, P.R. Fields, K. Rajnak, Electronic energy levels of the trivalent lanthanide aquo ions. II. Gd^{3+}, J. Chem. Phys. 49 (1968) 4424–4442, https://doi.org/10.1063/1.1669893.
[57] K.A. Naseer, S. Arunkumar, K. Marimuthu, The impact of Er^{3+} ions on the spectroscopic scrutiny of Bismuth bariumtelluroborate glasses for display devices and 1.53 μm amplification, J. Non-Cryst. Solids 520 (2019), 119463, https://doi.org/10.1016/j.jnoncrysol.2019.119463.
[58] E. Şakar, Ö.F. Özpolat, B. Alım, M.I. Sayyed, M. Kurudirek, Phy-X/PSD: development of a user friendly online software for calculation of parameters relevant to radiation shielding and dosimetry, Radiat. Phys. Chem. 166 (2020), 108496, https://doi.org/10.1016/j.radphyschem.2019.108496.